Bulletin of the Seismological Society of America, Vol. 93, No. 6, pp. 2737–2751, December 2003

Estimated Ground Motion From the 1994 Northridge, California, Earthquake at the Site of the Interstate 10 and La Cienega Boulevard Bridge Collapse, West Los Angeles, California

by David M. Boore, James F. Gibbs, William B. Joyner,* John C. Tinsley, and Daniel J. Ponti

Abstract We have estimated ground motions at the site of a bridge collapse during the 1994 Northridge, California, earthquake. The estimated motions are based on correcting motions recorded during the mainshock 2.3 km from the collapse site for the relative site response of the two sites. Shear-wave slownesses and damping based on analysis of borehole measurements at the two sites were used in the site response analysis. We estimate that the motions at the collapse site were probably larger, by factors ranging from 1.2 to 1.6, than at the site at which the ground motion was recorded, for periods less than about 1 sec.

Introduction

During the **M** 6.7 Northridge, California, earthquake of 17 January 1994, bridges at two sites along the interstate highway I-10 corridor in the western part of Los Angeles collapsed or suffered major damage (Caltrans, undated). Both sites at which the bridges suffered major damage or collapse are underlain by considerably thicker Holocene deposits than those underlying nearby bridges that suffered minor to moderate damage. We focus on the intersection of I-10 with La Cienega Boulevard, at which overpass bridges collapsed (we refer to this as the I-10 site); other similarly built overpasses along the highway within several kilometers did not collapse. There are geological reasons to believe that the near-surface materials are softer at the collapse site than at nearby sites (*ciénaga* means "marsh" in Spanish). The I-10–La Cienega Boulevard intersection is located approximately 24 km southeast from the epicenter of the Northridge earthquake (Fig. 1). No strong-motion records were obtained at this site during the Northridge mainshock. The nearest strong-motion instrument that recorded the mainshock, Saturn Street School (USC91), is located 2.3 km northeast of the bridge site (Anderson *et al.*, 1981) (Fig. 1). Subsequent to the earthquake, several boreholes were drilled at the I-10 site (Darragh *et al.*, 1997) and one borehole was drilled at Saturn Street School. The boreholes have been logged using various methods. We interpreted the borehole measurements to obtain near-surface shear-wave slownesses and damping, and we used this information to estimate the ground motion during the mainshock at the I-10 site by correcting the recorded ground motion at Saturn Street School for the relative site responses at the two sites, using both linear and equivalent-linear approximations to nonlinear soil response calculations. We find that the ground motions at the I-10 site were probably larger, by factors ranging from 1.2 to 1.6, than at the Saturn Street School site for periods less than about 1 sec, although inherent spatial variability does not allow us to be certain of this. We speculate that this difference in ground motion contributed to the localized collapse of the bridges at the I-10 site.

Near-Surface Slownesses and Attenuation

The basis for the estimates of ground motion at the I-10 site is to deconvolve the recorded motion at Saturn Street School by the local site response and then convolve this input motion with the site response at the I-10 site. This procedure requires shear-wave slownesses and attenuation beneath both sites. In this section we describe how the models used in the calculations were constructed.

We use slowness rather than velocity (the two are reciprocals of one another), because differences in site amplification are most sensitive to differences in the near-surface seismic velocities; plots of slowness emphasize these near-surface differences better than plots of seismic velocity. Plots of seismic velocities tend to be dominated by the higher velocities in a profile, and what may appear to be significant differences in velocities between two sites are often not reflected in differences in site response. In general, the amplification will be higher at sites with larger slowness near the surface. Furthermore, most slownesses are estimated directly from data as the slope of a line fit to travel time as a function

*Deceased, 24 March 2001.

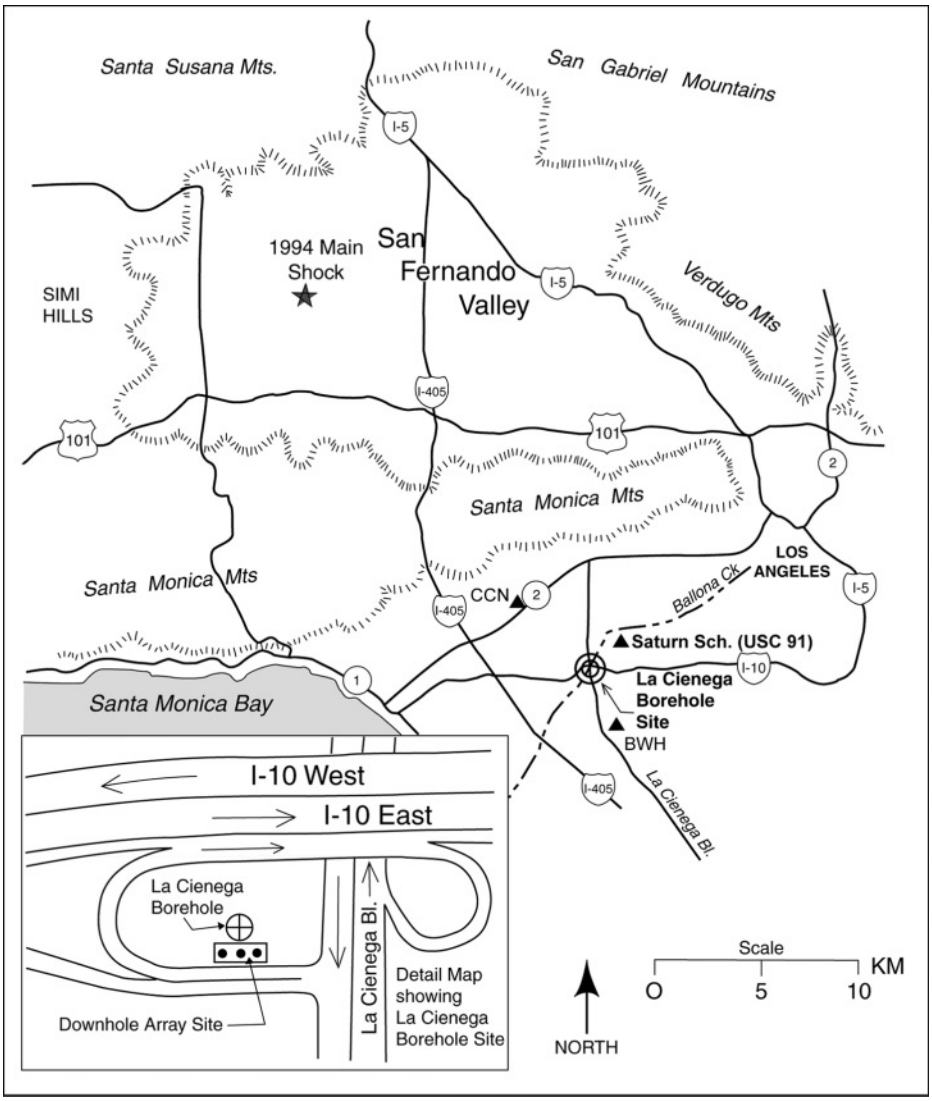

Figure 1. Location of the borehole at La Cienega Boulevard and Interstate 10 relative to the Northridge earthquake epicenter. The borehole is located at 34.0364° N and 118.3780° W (NAD83 datum). The Saturn Street School site (USC91) and two other sites (BWH and CCN) from which data are used in this article are indicated by triangles.

of depth; seismic velocity values traditionally reported are simply the inverse of the slopes of the fitted lines.

Shear-Wave Slownesses

We used seismic slownesses derived from measurements made using two borehole logging methods: surface-to-borehole (s2b) logging and suspension logging. We did the s2b logging and are reporting the results for the first time here. The s2b method (Warrick, 1974) uses recordings on a transducer clamped at various depths in the borehole using a surface source described by Liu *et al.* (1996). A record section is constructed of the recorded waveforms, and first-arrival times are picked from the resulting record section; these arrival times are fit using a model with constant-slowness layers. Details of the measurement and interpretation methods are given in the U.S. Geological Survey Open-File Reports describing the results from many boreholes (e.g., Gibbs *et al.*, 2000). For the I-10 hole the waveforms are very clean (Fig. 2), making it easy to pick the first-arrival times. The lithology, *SP* logs, resistivity logs, and derived shear-wave velocity for the I-10 site are given in Figure 3; tables of the shear-wave and the compressional-wave velocities are given in Boore (2003).

Results from the suspension logging method were obtained from measurements and analyses performed by the Resolution of Site Response Issues from the Northridge Earthquake (ROSRINE) project (http://geoinfo.usc.edu/rosrine) and by the California Department of Transportation (Caltrans) (C. Roblee, personal comm., 1999). The suspension logging method uses a probe, containing both a source

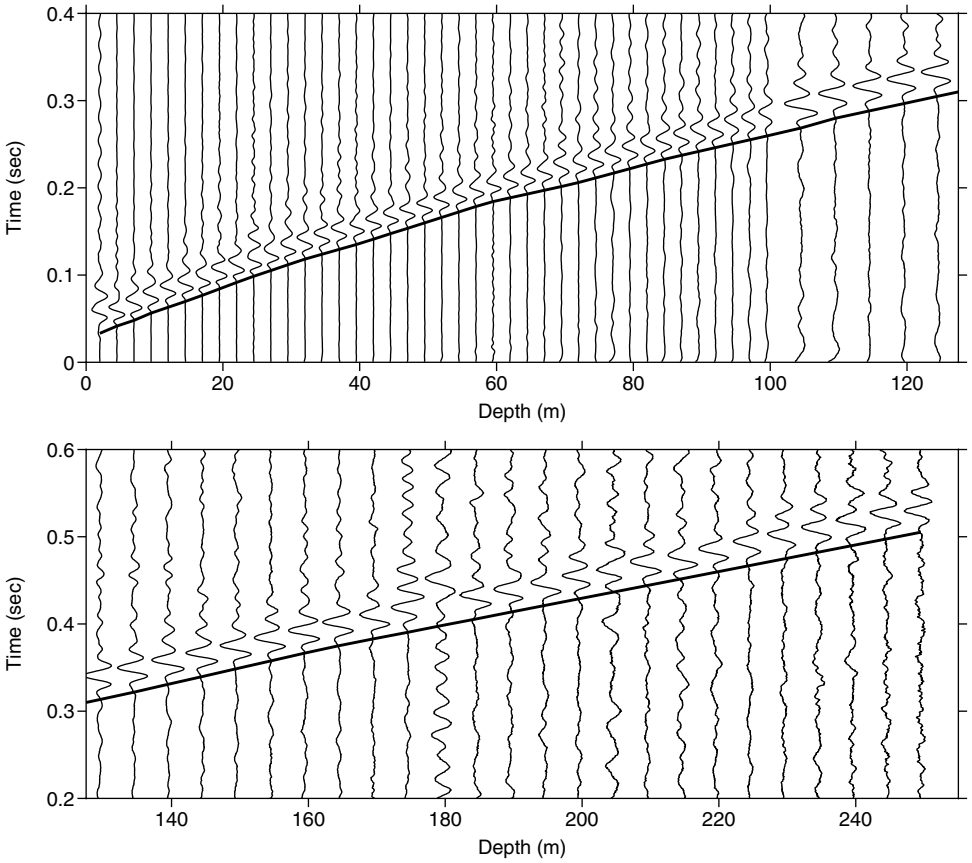

Figure 2. *S*-wave recordings for one horizontal direction for the surface-to-borehole logging done at I-10–La Cienega. The waveforms have been rotated and filtered with a 30-Hz low-cut Butterworth causal filter. The amplitudes have been individually scaled; the scaling changes when the spacing between recordings changed from 2.5 to 5.0 m at 100 m. The times in the bottom panel start at 0.2 sec, but the scaling of time is the same in both panels. The times are relative to the impact at the source, offset 5 m horizontally from the borehole. The heavy solid line is the calculated travel time from the model obtained by fitting first arrivals picked on the waveforms.

and receivers, that is lowered into the borehole (Nigbor and Imai, 1994). Interval slownesses are obtained between the receivers, 1 m apart, for a series of depths down the hole. The slownesses from the ROSRINE project at the I-10 site are for depths between 26 and 278 m (Fig. 3); the Caltrans logging provided slownesses from 1.5 to 95.6 m (Fig. 4a). At the Saturn site the ROSRINE measurements were made between 1.5 and 97 m; these results are given in Figure 4b. Caltrans measurements were not made at the Saturn site.

The suspension logging data are basically point estimates of the slowness, and they do not extend to the surface. For purposes of computing site amplifications, however, it is desirable to have a model of seismic slownesses made up of a stack of constant slowness layers. We have derived such models from the suspension logging data by computing the effective slowness for a set of depths corresponding to a layered model. The travel time across each layer was computed using

$$t_n = \sum_{i=1}^{n} s_i d_i, \tag{1}$$

where s_i is the slownesses from the suspension logging data, d_i is the spacing between suspension logging measurements, and n is the number of measurements in the layer. The equivalent slowness for the layer was computed from

$$s_{\text{lyr}} = \frac{t_n}{d_{\text{lyr}}}, \tag{2}$$

where s_{lyr} is the average slowness in the layer and d_{lyr} is thickness of the layer. The missing top 1.5 m from the suspension logs was assumed to have the value of slowness measured at 1.5 m.

We constructed four models from the available suspension data: two models at I-10–La Cienega and two at Saturn

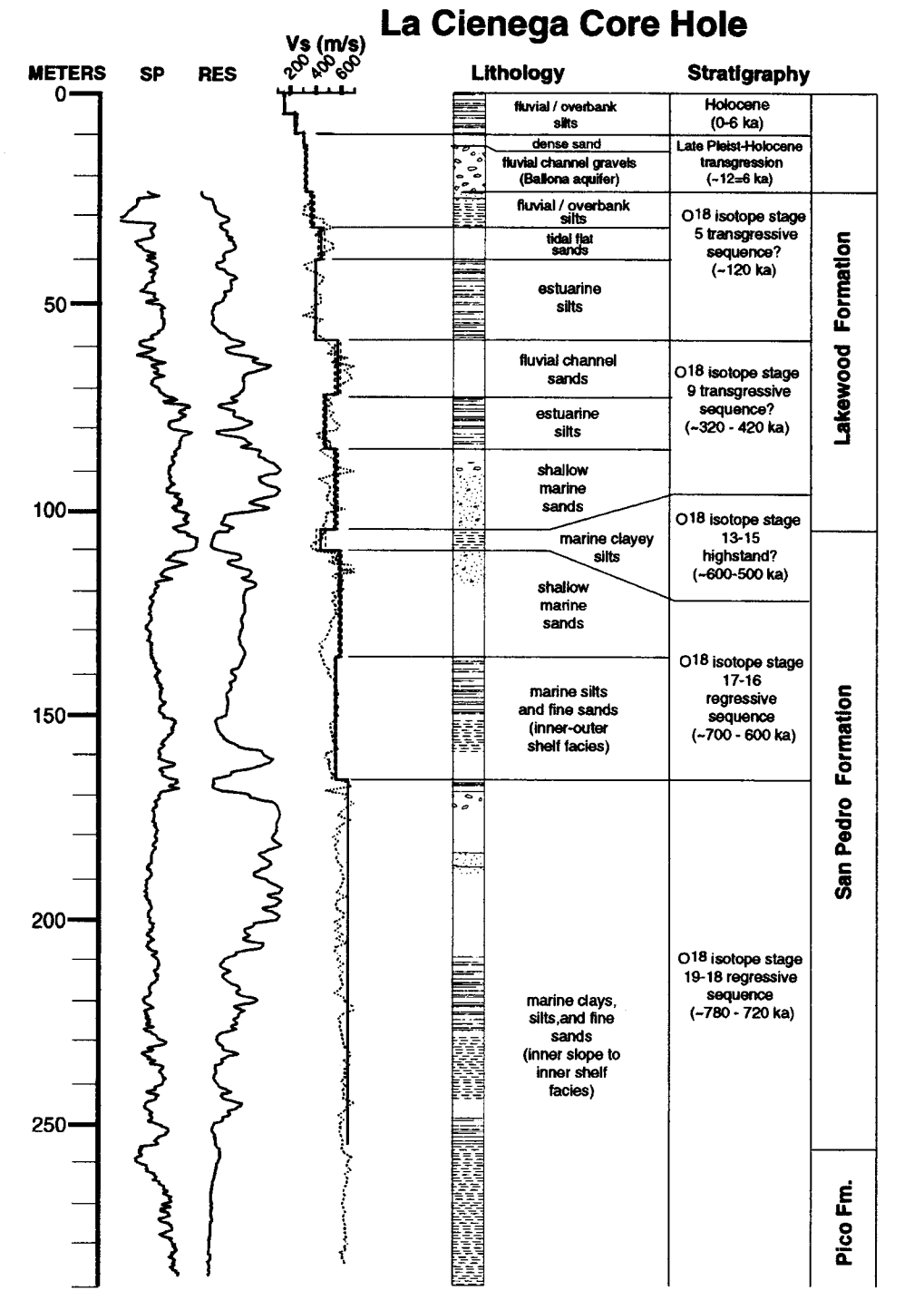

Figure 3. Simplified lithology for the core borehole located approximately 4 m south of the hole logged for velocities. The upper 80 m are nonmarine sediments. The top 5 m have an average *S* velocity of 163 m/sec, and the average *S* velocity to a depth of 12.5 m is 208 m/sec. Shear-wave velocity profiles (suspension logging data, dotted; s2b logging, solid line) are shown with two electric logs. The upper portion (23 m, 75 ft) of the borehole had to be surface cased to prevent cave-in while drilling, precluding electric logs and suspension logging from obtaining data in the top part of the borehole (but suspension logging measurements were made at these shallower depths in a nearby borehole) (see Fig. 4).

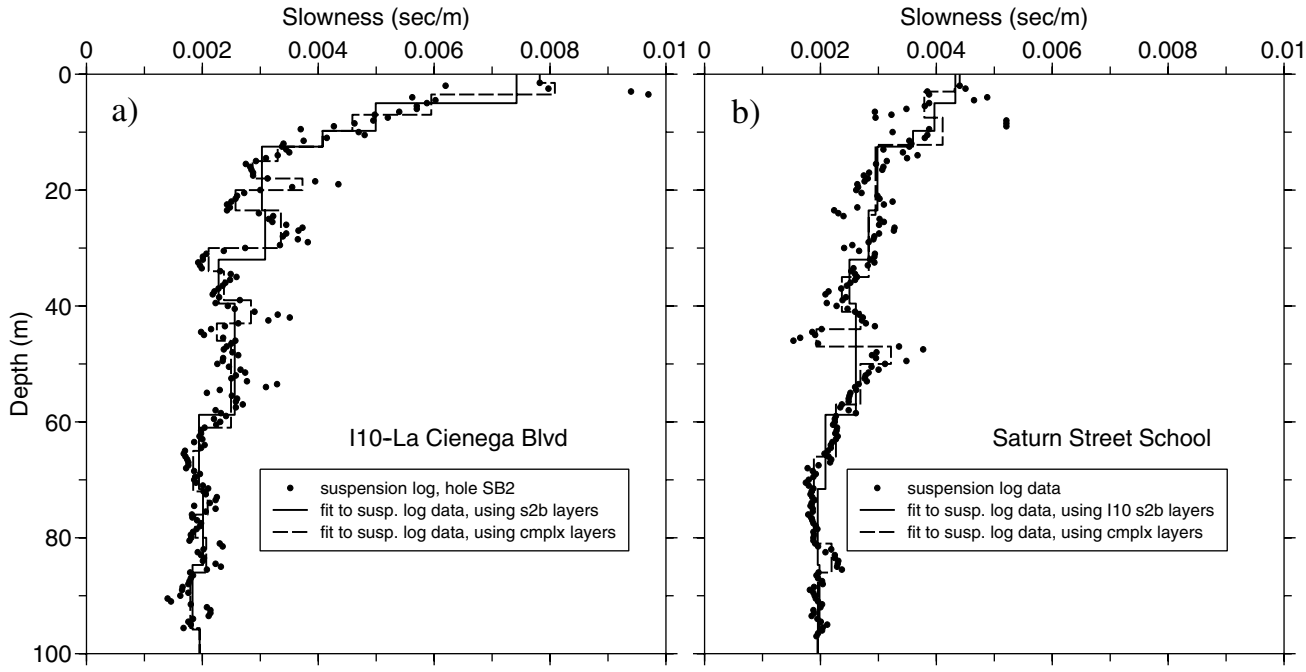

Figure 4. Slowness from suspension log data, compared to layered models fit to that data using two layered models: "s2b" (surface to borehole) uses the layering derived from the analysis of the surface-to-borehole logging of a borehole at I-10, and "cmplx" uses more detailed layering guided by the suspension log data. (a) I-10–La Cienega data models; (b) Saturn Street School data and models. Models have the same depth interfaces below 100 m. The suspension log data were obtained from http://geoinfo.usc.edu/rosrine and from C. Roblee (private comm., 1999).

Street School. The models differ only in the choice of layering. Layering was chosen based on subjective inspection of the suspension logging data for each site separately; this layering generally has more detail than from interpretations of the s2b logging and the resulting models are termed the "complex" models. In addition, the layering of the model derived from the s2b measurements at I-10 was used for averaging the suspension logging data at both the I-10 and Saturn Street School sites; these models are termed "s2b" models. A comparison of the slownesses for these layered models and the suspension logging data are given in Figure 4.

For site response calculations, it is desirable to have a velocity model that extends to depths great enough to influence the site response at the lowest frequencies of interest. We want to compute site response for frequencies down to about 0.5 Hz; for the I-10 site, the maximum depth (250 m) corresponds to a quarter wavelength at a frequency of 0.5 Hz. Unfortunately, the velocities at the Saturn site are only available to about 100 m. Given the proximity of the two sites and the similarity of their slownesses below about 12.5 m (Fig. 4), however, we decided to assume that the slownesses at depths greater than 97 m at the Saturn site are the same as at the I-10 site. This assumption affects frequencies less than about 0.9 Hz.

A comparison of all layered models is given in Figure 5, from which it can be seen that the slownesses near the surface at I-10 are consistently higher than at Saturn Street School. (The models, in terms of velocity, are tabulated in Table 1.) In addition, the suspension logging slownesses at I-10 are higher than from the s2b models. Finally, the models for both I-10 and Saturn Street School are similar at depths below about 12.5 m. The site amplifications shown later will reflect all of these features.

The larger S slowness at the I-10 site reflects the appreciable thickness (10 m) of rather soft Holocene alluvium at that site. These sediments were deposited when the sea level rose as the last ice age abated, mainly in the interval from about 13,000 to 6,000 years before present. In contrast, Saturn Street School is located on the northern margin of the Ballona Creek floodplain where the Holocene deposits are very thin, persistent swamps were absent, and the Holocene overlies moderately dense Pleistocene alluvium, a distinctively different near-surface site condition than at the I-10 site.

Damping Factor D_s

The site amplification functions used in our deconvolution/convolution procedure require, in addition to shear-wave slowness, an estimate of the damping factor D_s. In seismology, damping is more often measured by the quality factor Q, although the damping factor is the more natural

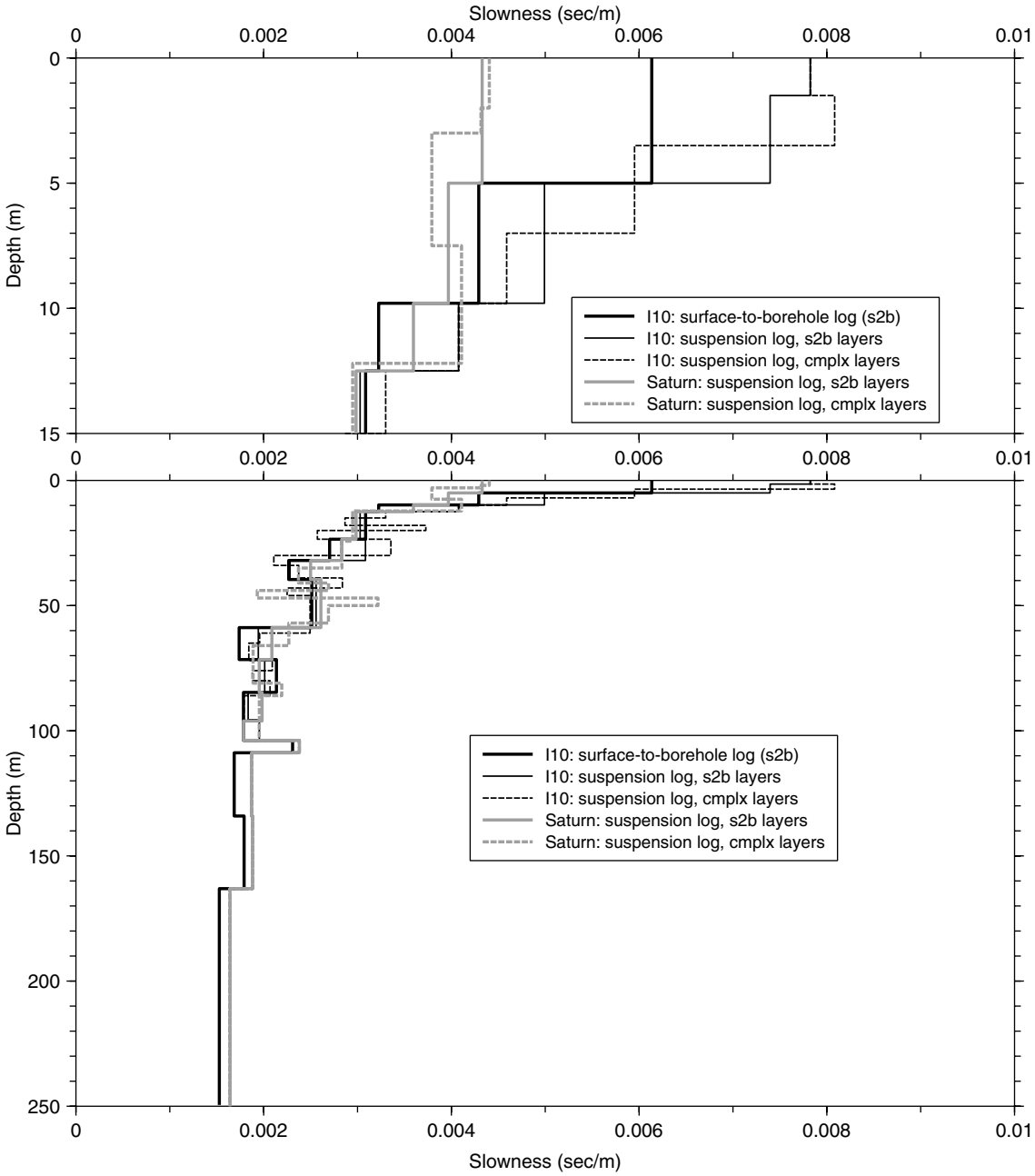

Figure 5. Comparison of slowness models determined from s2b and suspension log data. The black and gray lines are models for I-10 and Saturn Street School, respectively. Two models based on the suspension log data are used, using different layering (see caption of Fig. 4 for explanation of s2b and cmplx). The upper panel gives details within 15 m of the surface, where the various models differ the most. These differences control the variations in amplification. Although not obvious in the figure, the curves for all but the I-10 surface-to-borehole log are the same below about 105 m.

quantity to use. The two factors are related by the simple equation $Q_s = 0.5/D_s$. The quality factor Q is defined as $2\pi E/\Delta E$, where ΔE is the energy lost through anelastic processes in a cycle of deformation and E is the peak energy stored in the cycle (Aki and Richards, 1980). Loosely speaking, Q is the number of wavelengths of propagation required for anelastic attenuation to reduce the amplitude of a wave by a factor of $e^{-\pi}$. We measured the shear-wave damping factor D_s by the method described by Gibbs *et al.* (1994) with minor modifications. Briefly, a preliminary value of D_s for each frequency f is obtained by correcting the natural logarithm of the shear-wave spectral amplitude for geometric spreading and for the effects of changes in the shear-wave impedance and then regressing the corrected amplitude

Table 1
Velocity Models Used in Calculations*

I-10–La Cienega						Saturn Street School			
surface-to-borehole		susp. log: s2b layering		susp. log: cmplx layering		susp. log: s2b layering		susp. log: cmplx layering	
d2b	V_s	d2b	V_s	d2b	V_s	d2b	V_s	d2b	V_s
5.0	163.0	1.5	127.8	1.5	127.8	5.0	231.0	2.0	227.0
9.8	233.0	5.0	135.2	3.5	123.7	9.8	252.0	3.0	231.7
12.5	310.0	9.8	200.3	7.0	168.0	12.5	278.0	7.5	263.7
23.5	324.0	12.5	245.3	9.8	217.9	23.5	335.0	12.2	243.4
32.0	370.0	23.5	330.2	12.5	245.3	32.0	353.0	24.3	339.0
39.6	441.0	32.0	324.1	15.0	303.0	39.6	400.0	35.0	352.8
58.8	398.0	39.6	438.3	18.0	348.8	58.8	383.0	41.0	421.8
71.6	575.0	58.8	390.8	20.0	268.2	71.6	479.0	44.0	371.5
84.7	468.0	71.6	514.6	23.5	388.6	84.7	512.0	47.0	517.3
103.9	560.0	84.7	497.0	30.0	298.0	96.1	504.0	50.0	310.7
108.8	433.0	95.6	545.0	34.0	474.3	103.9	560.0	57.0	371.6
134.1	593.0	103.9	511.5	39.0	421.1	108.8	420.0	66.0	440.9
163.1	558.0	108.8	420.0	43.0	352.2	134.1	534.0	81.0	529.7
249.5	654.0	134.1	534.7	46.0	444.3	163.1	531.0	86.0	455.9
		163.1	531.4	61.0	400.7	250.0	609.0	97.0	511.4
		250.0	608.9	65.0	510.9			103.9	512.0
				72.0	542.8			108.8	420.0
				76.0	477.9			134.1	534.7
				80.0	532.1			163.1	531.0
				86.0	483.5			250.0	608.9
				95.6	557.8				
				103.9	512.0				
				108.8	420.0				
				134.1	534.7				
				163.1	531.0				
				250.0	608.9				

*d2b = depth to bottom of layer in m; V_s = shear-wave velocity in m/sec.

value against shear-wave travel time. The preliminary value of D_s is obtained from the regression coefficient, which is equal to $-2\pi f D_s$. In order to correct for wave propagation effects, particularly reflections at layer boundaries, synthetic seismograms are generated using a computer program written by Herrmann (1996). This is a complete wave-propagation program that uses wavenumber integration and a layered Earth model; the calculations include near-field terms and all interbed reflections. Synthetic seismograms are computed using the same slowness model as used in the analysis of the data and a damping value that is an average of those from the initial analysis. The synthetic seismograms are processed in the same way as the recorded seismograms, and the difference between the derived damping and the value used in the calculations is used to correct the values from the analysis of the data. In all cases the corrections derived from the synthetic seismograms were small. Our computer programs for calculating D_s have an option that permits us to impose the condition that D_s is independent of frequency and calculate the value that best fits the data at all frequencies considered.

Applying this method to the s2b data from the I-10–La Cienega site (shown in Fig. 2) gives the results shown in Figure 6. There is relatively little frequency dependence over the range of the measurement, and the average D_s, from the frequency-independent assumption over the depth range from 0 to 220 m, is 0.012. This value of D_s is slightly low compared to those we have obtained at other sites in California with comparable velocities and fine-grained soils; these other dampings are generally between 0.014 and 0.020. We assume that the damping factor of 0.012 also applies to the Saturn site. The damping factor depends on soil type as well as overall average velocity (J. Gibbs *et al.*, unpublished results); according to the geotechnical logs available from http://geoinfo.usc.edu/rosrine, as well as those shown in Figure 3, the soils under both sites are similar, being a mix of clays, silts, and sands. For this reason we feel justified in using the same damping for both sites.

Estimate of Ground Motions at the I-10–La Cienega Site

The procedure for estimating the ground motion at the I-10–La Cienega site from the recorded motion at Saturn Street School is based on deconvolving the observed motion at the Saturn site to obtain the equivalent input motion at the base of the 250 m stack of layers and then using this motion as input into the 250 m stack of layers beneath the I-10 site to compute the surface ground motion at that site. We have done the calculations assuming both linear and an equiva-

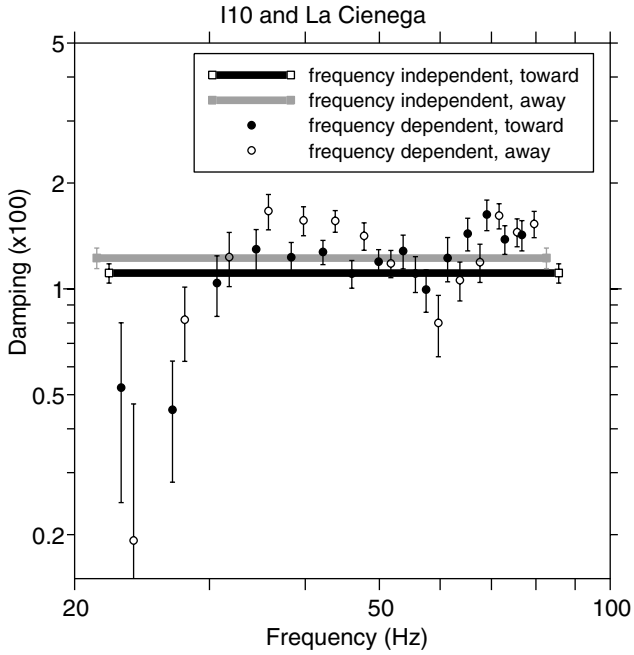

Figure 6. Shear-wave damping D_s, multiplied by 100 (to give percent damping; $D_s = 0.5/Q_s$, where Q_s is the quality factor), averaged over a depth range of 0–220 m, calculated from the decay of amplitude with depth. Horizontal lines represent D_s derived under the assumption of frequency-independent damping. Two suites of waveforms used to derive the damping were obtained, one by driving the surface shear-wave source in one direction (toward) and the other by driving the source in the opposite direction (away). The near horizontal trend of the values supports the constant D_s assumption over most of the frequency range. The average of the values represented by the two horizontal lines was used in the site amplification calculations.

lent-linear approximation to nonlinear response. The procedures and results of each are described in turn.

Linear Calculations

By assuming that the system is linear, the step of deriving the deconvolved time series beneath the Saturn site can be dispensed with, and the Fourier spectra of the surface motion at the I-10 site can be written as

$$A_{I10}(f) = \frac{S_{I10}(f)}{S_{Sat}(f)} A_{Sat}(f), \quad (3)$$

where $A_{I10}(f)$ and $A_{Sat}(f)$ are the Fourier spectra of the estimated motion at the I-10–La Cienega site and the recorded motion at the Saturn Street School site, respectively (we use the 110° horizontal-component motion at Saturn Street School in the analysis). $S_{Sat}(f)$ and $S_{I10}(f)$ are the site amplification functions (including amplitude and phase) at Saturn Street School and I-10–La Cienega, respectively, relative to the motions for a model in which the top 250 m of the soils at each site have been removed (i.e., the outcrop motion for the half-space beneath the stacks of layers). There is probably not a large impedance change in the vicinity of 250 m, so the results are not sensitive to the choice of depth corresponding to the half-space. Impedance changes at greater depths (such as at the interface between Quaternary and Tertiary deposits) will affect motions at longer periods than of interest here. Site amplifications for several of the layered models are shown in Figure 7. The site amplifications were computed assuming *SH* waves at an incidence angle of 10° from vertical (the results are not sensitive to this choice). The inverse Fourier transform yields an estimate of the ground acceleration time series at the I-10–La Cienega site. The motions at the I-10 site are larger than at the Saturn site for frequencies between about 1 and 10 Hz, as expected from the comparison of the slownesses in Figure 5. If the waves were not damped, the motions at I-10 would be larger than at Saturn for frequencies higher than 10 Hz as well; this is not the case, however, because of damping. Even though the damping value (a constant value for all layers) was the same for both I-10 and Saturn, the travel time is greater in the near-surface materials underlying I-10, and thus the effect of the damping on the high-frequency motions is greater at I-10 than at Saturn.

An important assumption in this analysis (and the nonlinear analysis to follow) is that the input motion obtained from deconvolving the site response at Saturn Street School is the same as the input motion below the I-10–La Cienega site. At first glance this seems to be a reasonable assumption, given the similarity of the soil profiles below 12.5 m (Fig. 5), the close separation of the two sites (2.3 km) compared to the distance to the source (about 24.5 km) (Fig. 1), and the similarity of the azimuths from the epicenter to the sites (318° and 323° for the Saturn Street School and I-10–La Cienega sites, respectively). Figure 8 shows the site amplification at both sites with the top 12.5 m of sediments removed. The two sites show very similar amplification with these sediments removed. We conclude that the path of the earthquake wavefront (amplitude and frequency content) was essentially the same as it swept through the two sites. In fact, the assumption that the seismic-wave input to the *S*-wave models was the same same at 250 m depth beneath the two sites may be the weakest assumption in this article; we discuss this in a separate section, just before the Summary and Discussion.

Nonlinear Soil Response

Trifunac and Todorovska (1996) found evidence for nonlinear soil response out to a maximum distance of 20 km from the epicenter of the Northridge earthquake at sites with soft soil conditions (which they defined as having average slowness over the upper 30 m between 0.003 and 0.006 sec/m; the average slowness at I-10 and Saturn over the upper 30 m is about 0.0040 and 0.0033 sec/m, respectively). They reported that at several strong-motion sites the peak horizontal amplifications were less than expected, and they at-

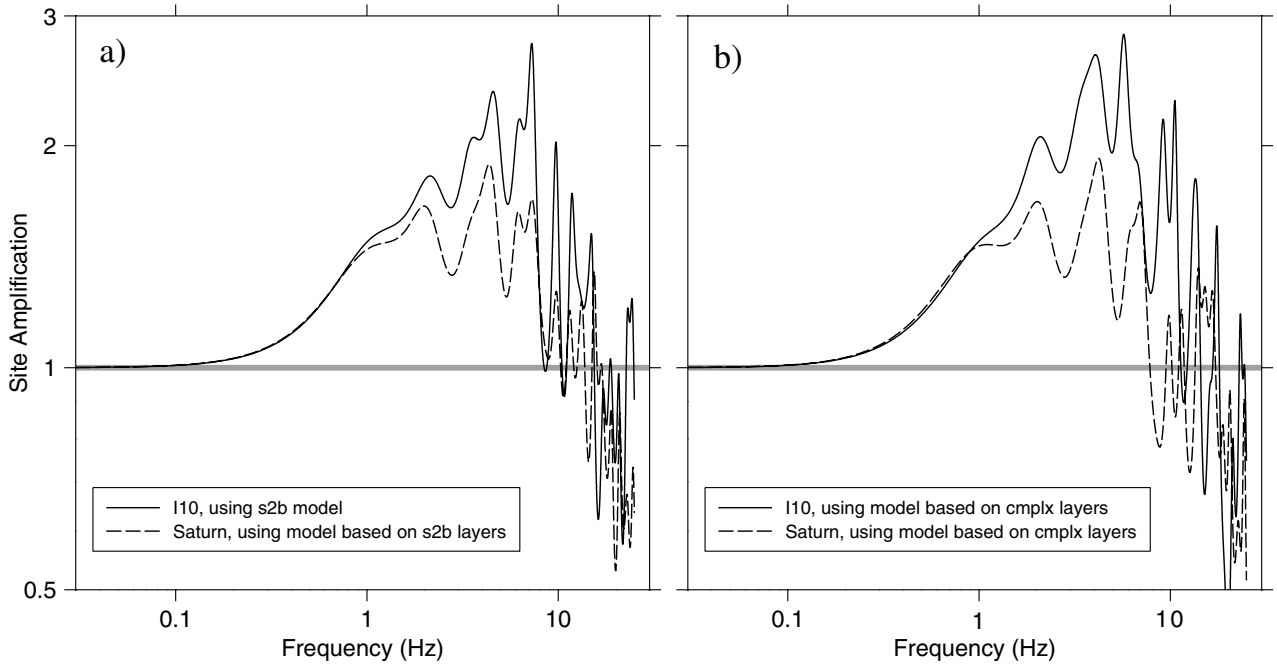

Figure 7. Site amplification at I-10–La Cienega and at Saturn Street School. Graphs (a) and (b) are for different layered models at the two sites (see caption of Fig. 4 for explanation of s2b and cmplx). Most of the amplification occurs between 1 and 10 Hz.

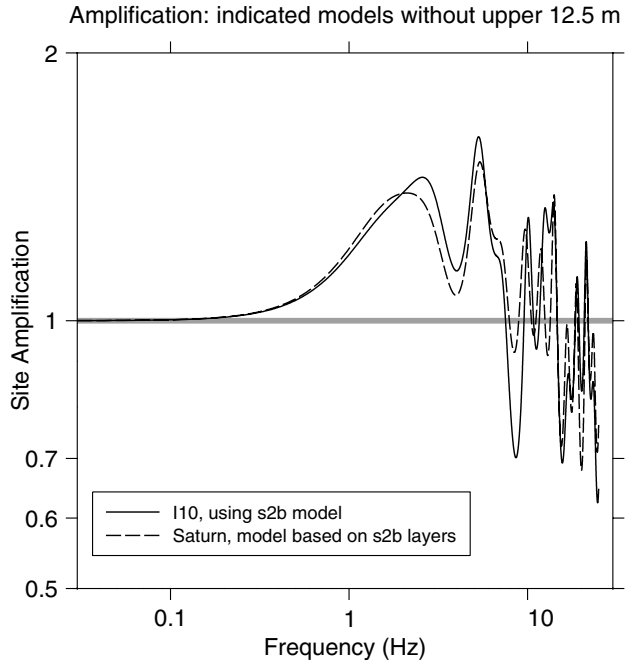

Figure 8. Site amplification at I-10–La Cienega (s2b) and at Saturn Street School. The top 12.5 m of sediments have been removed to compare the amplification response. Note change in vertical scale compared to Figure 7. The spectra show that the amplification from sediments below 12.5 m at the two sites is very similar.

tributed this to nonlinear soil response. Based on the relatively large peak acceleration and modest strain (as estimated from the peak velocity) recorded at Saturn Street School (station USC91, the station closest to the borehole site at I-10–La Cienega), Trifunac and Todorovska (1996) did not include the Saturn site as one for which the soil response was nonlinear during the Northridge earthquake. On the other hand, the nearby I-10 site has softer soils, with standard penetration blow counts from engineering borings of $N \approx 10$ (geotechnical logs from http://geoinfo.usc.edu/rosrine). In addition, utility-pipe breakage occurred close to the intersection of I-10–La Cienega, suggesting possible nonlinear ground displacement (although no sand boils, the usual evidence cited for liquefaction, were observed [Stewart *et al.*, 1996]). Finally, a number of studies have found evidence for widespread nonlinear soil response during the 1994 Northridge earthquake (e.g., Field *et al.*, 1997, 1998). For these reasons we thought it prudent to derive surface motions at the I-10 site assuming nonlinear soil response (at both sites).

We followed the procedure described in Cultrera *et al.*, (1999), using an equivalent-linear approximation of nonlinear wave propagation to deconvolve the recording at Saturn Street School, thus deriving the equivalent outcrop motions beneath the upper 250 m of the sediments. We used the program SHAKE91 (Schnabel *et al.*, 1972; Idriss and Sun, 1992) to deconvolve the motions at Saturn and to propagate these motions through the 250 m of sediments beneath the I-10 site to obtain the surface ground motions at the I-10

site. Although not doing true nonlinear calculations, the SHAKE91 program is widely used to compute the effects of nonlinear propagation, and the results are usually considered to give an adequate representation of truly nonlinear wave propagation, at least for frequencies up to about 10 Hz (W. Silva, personal comm.). For economy of expression, from here on we refer to SHAKE91 output as being the result of doing nonlinear calculations. The modulus reduction and damping curves used in the analysis were those recommended by Silva *et al.* (1996) for use in the Los Angeles region for cohesionless soils. For a given range of depths, these curves have less nonlinearity than the generic curves contained in EPRI (1993). To be specific, for depths between 0 and 15 m, the EPRI curves for depths of 16–46 m were used, and for depths greater than 15 m, the EPRI curves for the depth range 153–305 m were used. We also did the analysis by reducing the motions at the Saturn site so that the response would be essentially linear; the results were similar to those we obtained by doing the frequency domain analysis described earlier.

Results: Ratios of Response Spectra and Estimates of Motion at I-10

The result of both the linear and nonlinear calculations is a time series of ground acceleration at the I-10 site, so time series are available at both the I-10 and the Saturn sites. We thought that the most meaningful comparison of the motions would be provided by computing the response spectra for the motions at each site and then graphing the ratio of the response spectra from the two sites. We have done this and summarize the results in Figure 9. The shaded and hatched regions represent the range of ratios obtained using the six combinations of slowness models (three models are available at the I-10 site, one being the model from the s2b logging, and two from fitting the suspension logging data to two different sets of layers; and two models are available at the Saturn site, corresponding to the different assumptions about layering used in averaging the suspension logging results). In all cases, the response at the I-10–La Cienega site is greater than that at the Saturn Street School site for periods less than 1 sec. As expected from the slownesses shown in Figure 5, the largest difference is for the models based on the suspension logs. Even the smallest relative amplitude difference exceeds a factor of 1.2 for a wide period range. Interestingly, the nonlinear response predicts higher relative motions at the I-10 site than the linear model for periods greater than about 0.3 sec. This is undoubtedly due to the softening of the near-surface sediments produced by the relatively high strains in the layers (the modulus reduction in the upper 12 m at I-10 ranged from 0.36 to 0.51, with peak strains between 0.26% and 0.12%). The concurrent increase in damping (more than a factor of 6) is not enough to offset the increase in amplification due to the increase in slowness of the sediments. The absolute ground motions estimated for the I-10–La Cienega site are shown in Figure 10 for the range of linear and nonlinear calculations. We are not advocating that these motions be used in design, because of the effect of spatial variability, discussed next.

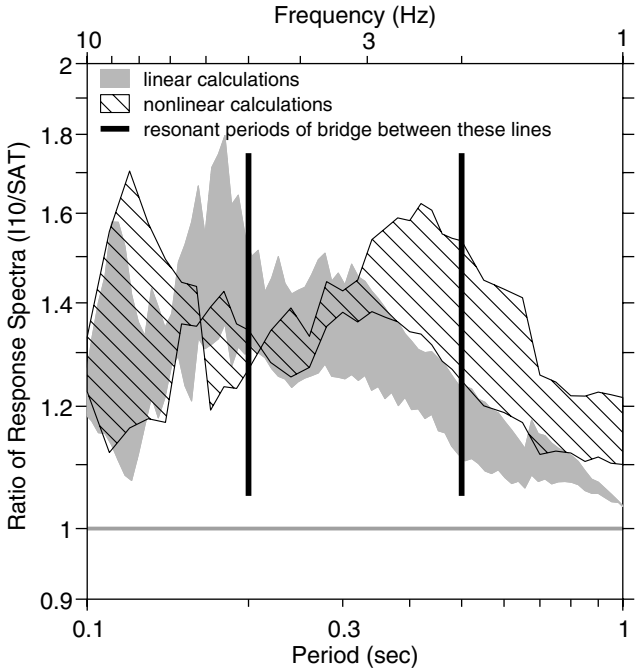

Figure 9. The 5% damped pseudo relative response spectra for ground motions at the I-10 site derived using linear and nonlinear soil response calculations, divided by the similar response spectrum of the recorded motion at the Saturn Street School site. The hatched and gray areas indicate the range of ratios; the areas are generally bounded by models in which the I-10 slowness is from the surface–source downhole-receiver (s2b) model (bottom of hatched and gray areas) and from the suspension log data (top of hatched and gray areas). As shown in Figure 5, the suspension logging slownesses are higher than the s2b slownesses near the surface, and that is why the ratio of site response is higher for the I-10 model based on the suspension logging data. In all cases the response at the I-10 site is systematically higher than that at the Saturn Street School site for periods between 0.1 and 1 sec. The resonant period of the bridge structure at I-10–La Cienega is estimated to lie between the vertical lines (C. Roblee, private comm., 1997).

Effect of Spatial Variability of Ground Motions

A number of studies find that waveforms of motions having frequencies above about 1 Hz rapidly lose coherence as station spacing increases, even for stations on sites with apparently similar surficial geology (e.g., Abrahamson, *et al.*, 1991; Hough and Field, 1996). Other studies find a significant increase in the variability of ground-motion amplitudes as a function of station spacing (e.g., Abrahamson and Sykora, 1993; Steidl, 1993; Field and Hough, 1997). These latter studies are of particular importance regarding our as-

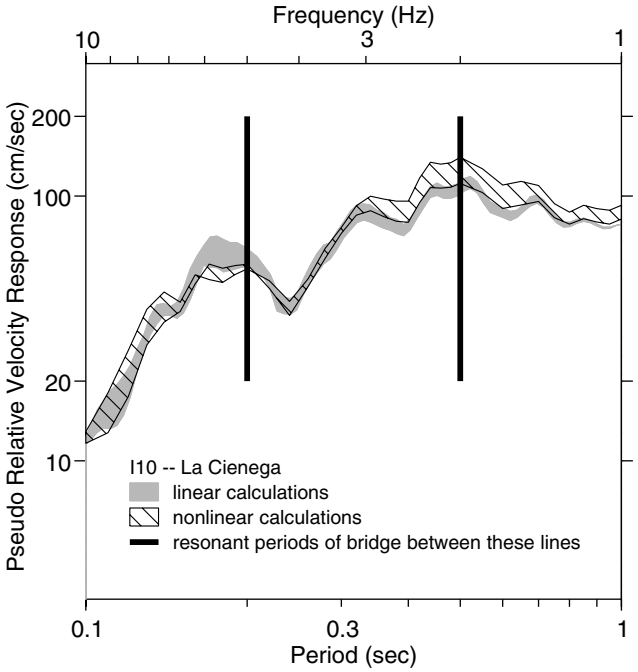

Figure 10. The 5% damped pseudo relative response spectra for ground motions at the I-10 site derived using linear and nonlinear soil response calculations. The hatched and gray areas indicate the range of ratios; the areas are generally bounded by models in which the I-10 slowness is from the surface-source downhole-receiver (s2b) model (bottom of hatched and gray areas) and from the suspension log data (top of hatched and gray areas). The resonant period of the bridge structure at I-10–La Cienega is estimated to lie between the vertical lines (C. Roblee, written comm., 1997).

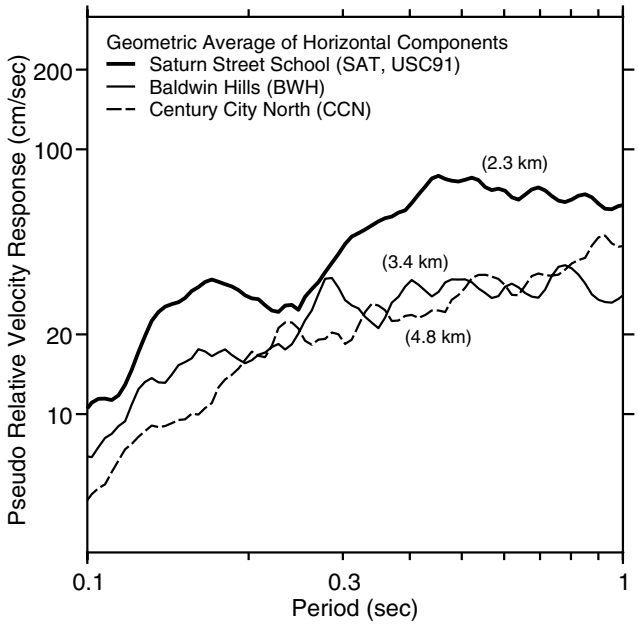

Figure 11. The 5% damped pseudo relative response spectra for ground motions at Saturn Street School, Baldwin Hills, and Century City–LACC North. The latter two sites have been corrected for geometrical spreading to the distance to Saturn Street School, using the equations of Boore *et al.* (1997). Shown are the geometrical means of the two horizontal components of the spectra computed from the motions recorded at each station. The distance from each station to the I-10–La Cienega are given in parentheses.

sumption that the deconvolved motion beneath Saturn is similar to the input motion under I-10. Coherency is of less concern than overall differences in amplitude, because the various combinations of velocity models and the use of equivalent linear rather than true nonlinear calculations means that the detailed phasing of the input motion will not influence the overall level of ground motion calculated at I-10. If the spatial variability were large enough it is possible that the input motion beneath I-10 could have been so small relative to that beneath Saturn that the surface motions at I-10 could have been smaller than at Saturn, even after amplification due to wave propagation through the sediments under I-10. This is what we discuss in this section.

One way of assessing variability is to compare motions recorded at other stations. Three stations within a radius of 5 km of I-10 recorded the 1994 Northridge mainshock (see Fig. 1 for locations). Figure 11 shows the geometrical mean of the response spectra from these three stations. The spectra for Baldwin Hills (BWH) and Century City–LACC North (CCN) have been corrected to the source-to-site distance of Saturn (an average factor of 1.11 and 0.82 for BWH and CCN, respectively) using the equations of Boore *et al.* (1997). As shown in Figure 11, there are large differences between Saturn and the other two sites. Velocities from *P-S* suspension logging are available from BWH, and these are very similar to those from Saturn Street School (Fig. 12). We could use these other motions as input to the velocity model under I-10, and in terms of absolute motions the results would be similar to multiplying the ordinates in Figure 11 by the amplification factors in Figure 9 (of course, the nonlinear amplifications would not be the same, but in view of the variability and the fact that we are not advocating any particular motion for design, the overall level of motions would not change). Because Saturn is the closest station, and also because the geographic setting is similar to that at the I-10 site (not near the edge of mountains, as is CCN, and not in a hilly area, as is BWH), we consider the motions at Saturn to be more appropriate than the other two motions as input. We recognize, however, that variability can still exist in the motions over a distance of 2.3 km. The rest of this section quantifies this variation and uses it to estimate a range of motions at I-10.

Most studies of variability used smaller earthquakes than the 1994 Northridge mainshock and usually consider more than one earthquake; both of these factors can contribute to an overstatement of the variability expected for motions from the Northridge mainshock (e.g., Abrahamson and

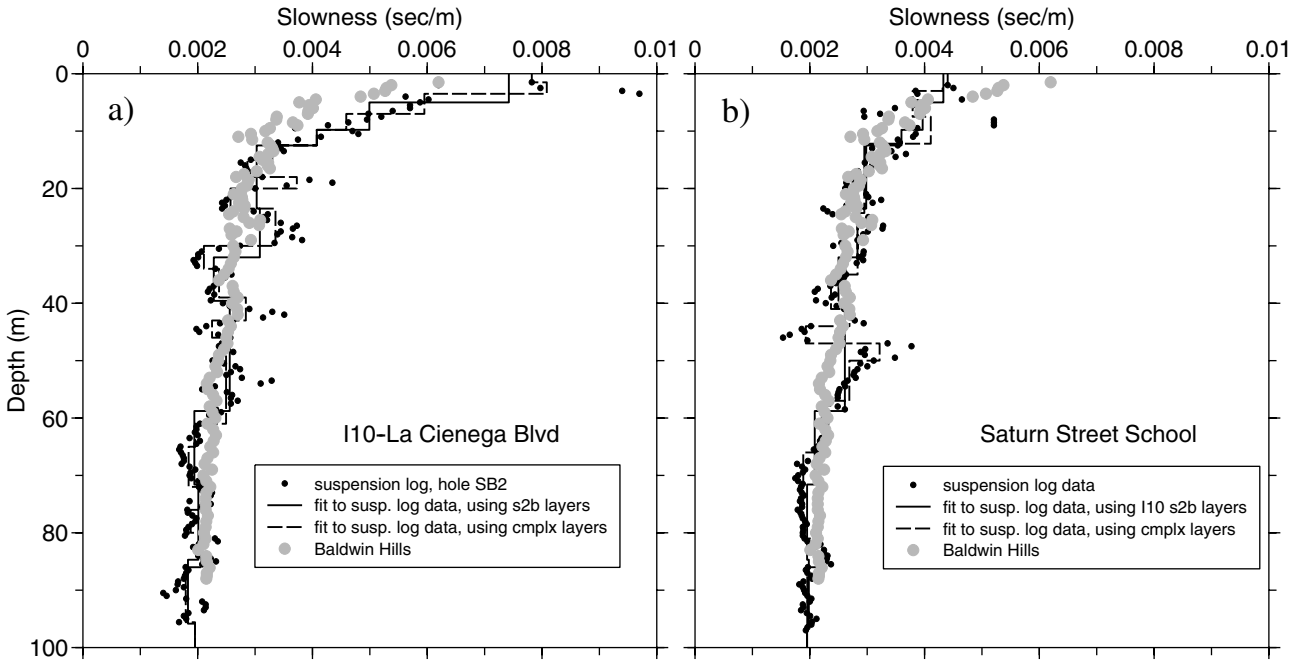

Figure 12. Slowness from suspension log data at Baldwin Hills compared to layered models fit to slowness data at the I-10–La Cienega and Saturn Street School sites (see caption to Fig. 4 for details).

Silva [1997], Campbell [1997], and Sadigh *et al.* [1997] found that the scatter about the regression fits to the data decreases with magnitude, and Field *et al.* [1992], Liu *et al.* [1992], Field and Hough [1997], and Baher *et al.* [2002] found that the variability depends on source location). For these reasons we present results of a study of variability of peak accelerations from the Northridge mainshock alone. These results were published by Boore (1997), but because the report in which the study appeared is not widely available, we repeat the details of that study in the Appendix.

The measure of variability is the standard deviation of the difference of the logarithm of peak motions for all pairs of stations whose interstation spacing falls into a distance bin chosen such that 15 station pairs are included in each bin. The results are shown in Figure A1. Also included in that figure are results from several small arrays, as well as the standard deviation about a regression curve for strong-motion data in the magnitude range 6.0–6.9. Because the application in this article is to estimate the variability of one motion given another, the standard deviations have been increased by a factor of $\sqrt{2}$ (this accounts for the fact that the observed motion might be lower or higher than the local mean of all data in a given interstation distance bin, and therefore the uncertainty of the predicted amplitude at another site, given the observed motion, should be greater than the variability about the local mean motion). Taken as a whole, the results clearly show that the variability increases rapidly with increasing station spacing. The results of Field and Hough (1997) are probably higher than those from the Northridge mainshock because they are studying a number of small earthquakes from a number of source locations. The most relevant results for our article are from the Northridge mainshock and the SMART1 array, the latter because the site geology is relatively uniform, whereas site geology was not accounted for in the study of the Northridge mainshock peak accelerations. For the 2.3-km distance between I-10 and Saturn, the results in Figure A1 suggest that the variability of one motion given the other is $10^{\pm 0.14}$ to $10^{\pm 0.18}$. (These variabilities are from observations at the ground surface, whereas we are interested in the variability of motions at a depth of 250 m. It is likely that a significant portion of ground-motion variability is due to changes in geology above this depth, but because we have no observations of spatial variability beneath the surface, we have used the conservative assumption that the spatial variability at the surface applies at depth.) For the important period range of 0.2–0.5 sec shown in Figure 9, the amplifications range from 1.1 to 1.6. Applying the variability factors to these amplifications results in the lowest amplification of 1.1 having a 68% chance of being between 0.7 and 1.7, and the highest amplification of 1.6 having a 68% chance of being between 1.1 and 2.4. The absolute ground motions in Figure 10 would be scaled accordingly. The results of doing this are shown in Figure 13, which can be thought of as roughly showing the 68% confidence limits of the motion at I-10. Thus the actual ground motions that occurred at I-10 during the 1994 Northridge mainshock could have been somewhat lower than the motions at Saturn, but overall it is more likely that they were amplified with respect to the motions at Saturn.

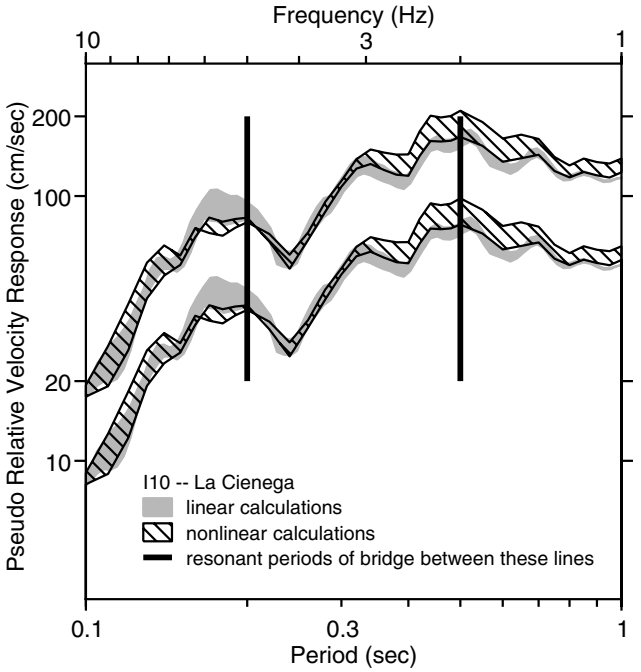

Figure 13. The 5% damped pseudo relative response spectra for ground motions at the I-10 site derived using linear and nonlinear soil response calculations, showing a range of estimates obtained by considering plus and minus one standard deviation of the amplitude of the input motion beneath I-10–La Cienega derived from the Saturn Street School recording. Within the context of this model and assumptions, the upper and lower sets of curves span the range within which there is roughly a 68% chance that the actual ground motion would be included. See the caption to Figure 10 for other details.

Summary and Discussion

We have made estimates of site amplification, pseudo relative velocity response, and acceleration values at I-10–La Cienega during the Northridge earthquake. Critical to these estimates is establishing the similarities/differences between the Saturn Street School site, where records of the mainshock exist, and the site at the I-10–La Cienega Boulevard intersection, where there are no mainshock records but where several bridges collapsed during the earthquake. Models based on shear-wave slowness measurements and lithology are compared at the two sites. Below 12.5 m depth the sites are nearly identical from a seismic response perspective. In view of the spatial variability in ground motion, we are not suggesting any particular motions to be used in engineering analysis of the bridge. We conclude, however, that the ground motions were probably higher at the I-10–La Cienega site than at the Saturn Street School site, particularly in the range of periods from 0.1 to 1.0 sec, and that this difference is mainly due to the softer sediments (higher *S* slowness) in the upper 12.5 m at the I-10–La Cienega site. The bridge support columns at I-10–La Cienega are located in these low-velocity sediments, and Caltrans engineers have estimated the resonant period of the bridge structures to be between 0.2 and 0.5 sec (C. Roblee, personal comm., 1997), which is in the range of the higher amplification at I-10–La Cienega. We therefore speculate that amplified shaking caused by soft ground conditions contributed to the damage and collapse of the highway structures at this site.

Acknowledgments

We thank Bob Darragh and Tony Shakal of the California Division of Mines and Geology for permission to make borehole measurements prior to installation of instruments at the La Cienega seismic array and Cliff Roblee and others at California Department of Transportation for engineering data and access to the site. We thank Bob Westerlund for help in the field; Tom Brocher, Bob Brown, Ken Campbell, Bob Darragh, John Ebel, and an anonymous reviewer for helpful comments on the manuscript; and Bob Simons for his wonderful program, CoPlot. John Evans provided a file with the Field and Hough (1997) results, and Hideji Kawakami and Hidenori Mogi graciously supplied a file with results from their paper. The linear site amplifications were computed using the program NRATTLE, written by Charles Mueller with modifications by Bob Herrmann.

References

Abrahamson, N. A., and W. J. Silva (1997). Empirical response spectral attenuation relations for shallow crustal earthquakes, *Seism. Res. Lett.* **68,** 94–127.

Abrahamson, N., and D. Sykora (1993). Variation of ground motions across individual sites, *Fourth DOE Natural Phenomena Hazards Mitigation Conf.*, Atlanta, Georgia, 19–22 October, 1993.

Abrahamson, N. A., J. F. Schneider, and J. C. Stepp (1991). Empirical spatial coherency functions for applications to soil-structure analyses, *Earthquake Spectra* **7,** 1–27.

Aki, K., and P. G. Richards (1980). *Quantitative Seismology Theory and Methods*, Vol. 1, W. H. Freeman, New York, 557 pp.

Anderson, J. G., M. D. Trifunac, T.-L. Teng, A. Amini, and K. Moslem (1981). Los Angeles vicinity strong motion accelerograph network, Civil Engineering Report CE 81-04, University of Southern California, 79 pp.

Baher, S., P. M. Davis, and G. Fuis (2002). Separation of site effects and structural focusing in Santa Monica, California: a study of high-frequency weak motions from earthquakes and blasts recorded during the Los Angeles Region Seismic Experiment, *Bull. Seism. Soc. Am.* **92,** 3134–3151.

Boore, D. M. (1997). Estimates of average spectral amplitudes at FOAKE sites, Appendix C in An evaluation of methodology for seismic qualification of equipment, cable trays, and ducts in ALWR plants by use of experience data, K. K. Bandyopadhyay, D. D. Kana, R. P. Kennedy, and A. J. Schiff (Editors), U.S. Nuclear Regulatory Commission NUREG/CR-6464 and Brookhaven National Lab BNL-NUREG-52500, C-1-C-69.

Boore, D. M. (2003). A compendium of *P*- and *S*-wave velocities from surface-to-borehole logging: summary and reanalysis of previously published data and analysis of unpublished data, *U.S. Geol. Surv. Open-File Rept. 03-191*, 13 pp.

Boore, D. M., W. B. Joyner, and T. E. Fumal (1997). Equations for estimating horizontal response spectra and peak acceleration from western North American earthquakes: a summary of recent work, *Seism. Res. Lett.* **68,** 128–153.

Caltrans (undated). The Northridge Earthquake Post Earthquake Investigation Report, California Department of Transportation, Division of Structures, 99 pp.

Campbell, K. W. (1997). Empirical near-source attenuation relationships

for horizontal and vertical components of peak ground acceleration, peak ground velocity, and pseudo-absolute acceleration response spectra, *Seism. Res. Lett.* **68,** 154–179.

Cultrera, G., D. M. Boore, W. B. Joyner, and C. M. Dietel (1999). Nonlinear soil response in the vicinity of the Van Norman Complex following the 1994 Northridge, California, earthquake, *Bull. Seism. Soc. Am.* **89,** 1214–1231.

Darragh, R. B., V. M. Graizer, and A. F. Shakal (1997). Site characterization and site response effects at CSMIP stations, Tarzana and La Cienega near the Santa Monica Freeway (I-10), California Strong Motion Instrumentation Program, OSMS 96-07.

Electric Power Research Institute (EPRI) (1993). Guidelines for Determining Design Basis Ground Motions, EPRI, Palo Alto, California, Rept. EPRI TR-102293, Vols. 1–5.

Field, E. H., and S. E. Hough (1997). The variability of *PSV* response spectra across a dense array deployed during the Northridge aftershock sequence, *Earthquake Spectra* **13,** 243–257.

Field, E. H., K. H. Jacob, and S. E. Hough (1992). Earthquake site response estimation: a weak-motion case study, *Bull. Seism. Soc. Am.* **82,** 2283–2307.

Field, E. H., P. A. Johnson, I. A. Beresnev, and Y. Zeng (1997). Nonlinear ground-motion amplification by sediments during the 1994 Northridge earthquake, *Nature* **390,** 599–602.

Field, E. H., Y. Zeng, P. A. Johnson, and I. A. Beresnev (1998). Nonlinear sediment response during the 1994 Northridge earthquake: observations and finite-source simulations, *J. Geophys. Res.* **103,** 26,869–26,883.

Gibbs, J. F., D. M. Boore, W. B. Joyner, and T. E. Fumal (1994). The attenuation of seismic shear waves in Quaternary alluvium in Santa Clara Valley, California, *Bull. Seism. Soc. Am.* **84,** 76–90.

Gibbs, J. F., J. C. Tinsley, D. M. Boore, and W. B. Joyner (2000). Borehole velocity measurements and geological conditions at thirteen sites in the Los Angeles, California region, *U.S. Geol. Surv. Open-File Rept. OF 00-470*, 118 pp.

Herrmann, R. B. (1996). Computer Programs in Seismology, Dept. of Earth and Atmospheric Sciences, Saint Louis University.

Hough, S. E., and E. H. Field (1996). On the coherence of ground motion in the San Fernando Valley, *Bull. Seism. Soc. Am.* **86,** 1724–1732.

Idriss, I. M., and J. I. Sun (1992). User's Manual for SHAKE91, Center for Geotechnical Modeling, Department of Civil and Environmental Engineering, University of California, Davis, November.

Kawakami, H., and H. Mogi (2003). Analyzing spatial intraevent variability of peak ground accelerations as a function of separation distance, *Bull. Seism. Soc. Am.* **93,** 1079–1090.

Liu, H.-P., R. L. Maier, and R. E. Warrick (1996). An improved air-powered impulsive shear-wave source, *Bull. Seism. Soc. Am.* **86,** 530–537.

Liu, H.-P., R. E. Warrick, R. E. Westerlund, E. D. Sembera, and L. Wennerberg (1992). Observation of local site effects at a downhole-and-surface station in the Marina District of San Francisco, *Bull. Seism. Soc. Am.* **82,** 1563–1591.

McCann, M. W., Jr., and D. M. Boore (1983). Variability in ground motions: root mean square acceleration and peak acceleration for the 1971 San Fernando, California, earthquake, *Bull. Seism. Soc. Am.* **73,** 615–632.

Nigbor, R. L., and T. Imai (1994). The suspension *P-S* velocity logging method, Proc. XIII International Conference on Soil Mechanics and Foundation Engineering, 5–10 January, 1994, New Delhi, India.

Sadigh, K., C.-Y. Chang, J. A. Egan, F. Makdisi, and R. R. Youngs (1997). Attenuation relationships for shallow crustal earthquakes based on California strong motion data, *Seism. Res. Lett.* **68,** 180–189.

Schnabel, P. B., J. Lysmer, and H. B. Seed (1972). SHAKE: a computer program for earthquake response analysis of horizontally layered sites, Earthquake Engineering Research Center, University of California at Berkeley, EERC 72-12.

Silva, W. J., N. Abrahamson, G. Toro, and C. Costantino (1996). Description and validation of the stochastic ground motion model, Final Report, Contract 770573, Brookhaven National Laboratory, Associated Universities, Inc. Upton, New York.

Steidl, J. H. (1993). Variation of site response at the UCSB dense array of portable accelerometers, *Earthquake Spectra* **9,** 289–302.

Stewart, J. P., R. B. Seed, and J. D. Bray (1996). Incidents of ground failure from the Northridge earthquake, *Bull. Seism. Soc. Am.* **86,** S300–S318.

Trifunac, M. D., and M. I. Todorovska (1996). Nonlinear soil response: 1994 Northridge, California, earthquake, *J. Geotechnical Eng. ASCE* **122,** 725–735.

Warrick, R. E. (1974). Seismic investigation of a San Francisco Bay mud site, *Bull. Seism. Soc. Am.* **64,** 375–385.

Appendix

Spatial Variability of Peak Accelerations from the 1994 Northridge Earthquake

This Appendix contains a summary of an analysis by Boore (1997) of the spatial variability of peak motion from the 1994 Northridge mainshock. The spatial variability in ground motions reduces to zero as the distance between two sites decreases to zero. On the other hand, for a great enough separation distance the spatial correlation of the ground motions reduces to zero and the additional uncertainty reaches that for an individual observation about the overall change of motion with distance (as given, for example, by fitting the data to a function using regression analysis). The two end-member cases suggests the following equation for the variance of peak ground motions as a function of intersite spacing (because ground motions are well approximated by a lognormal distribution, the standard deviations in the following discussion are those of the log of the ground motion; uncertainty ranges for the ground motion are given by multiplying and dividing the ground motion by 10 to the standard deviation):

$$\sigma^2_{\Delta \log Y} = \sigma^2_{\text{indobs}} \left(1 + \frac{1}{N}\right) F(\Delta)^2, \qquad \text{(A1)}$$

where $\sigma_{\Delta \log Y}$ is the standard deviation of differences in the logarithm of the peak motion Y, σ_{indobs} is the standard deviation of an individual observation about a regression, and N is the number of recordings used in the average of a group of recordings in a small region (the term in N accounts for the uncertainty in the estimate of the mean motion; for example, if one observation is available and the equation is to be used to compute how much another peak motion might vary as a function of spacing, $N = 1$). $F(\Delta)$ is a function that accounts for the spatial correlation of the motion, where Δ is the average separation between sites; F takes on values of 0.0 and 1.0 for $\Delta = 0$ and $\Delta = \infty$, respectively.

$F(\Delta)$ was estimated by studying larger peak horizontal accelerations from the 1994 Northridge mainshock, supplemented by studies of spatial variability in small arrays (Abrahamson and Sykora, 1993; Kawakami and Mogi, 2003), the SMART 1 array in Taiwan (N. Abrahamson, private comm., 1995; Kawakami and Mogi, 2003), and local regions in the

1971 San Fernando earthquake (McCann and Boore, 1983). The analysis for the Northridge data followed these steps:

1. Compute Δ for all pairs of stations, keeping only those for which the separation was less than 10 km (over 600 pairs).
2. For each pair, compute the difference of the logarithm of larger peak horizontal acceleration after correcting for differences in distance from the station to the earthquake (the distance attenuation used for this correction was derived in the course of the analysis as corrections to the average attenuation of Boore *et al.* [1997], although the results are insensitive to the particular attenuation equation that was used).
3. Divide the range of Δ into bins such that 15 station pairs are within each bin. This was done so that a reasonable estimate of the variance of the residuals could be obtained for each bin.
4. Compute the standard deviation of the residuals within each Δ bin.
5. Plot the standard deviations against the median distance for each bin, and fit a function to this plot, guided also by the Abrahamson and Boore and McCann studies. The results are shown in Figure A1. This procedure yielded the following equation for $F(\Delta)$:

$$F = (1 - \exp -\sqrt{0.6\Delta}). \qquad \text{(A2)}$$

Regression analyses of data for earthquakes with magnitudes between 6.0 and 6.9 finds that the within-earthquake standard deviation of individual observations about the mean (σ_{indobs}) is 0.188 and 0.182 for the larger and random horizontal peak acceleration, respectively (W. Joyner, personal comm., 1996). The results in Figure A1 are shown for the larger peak acceleration.

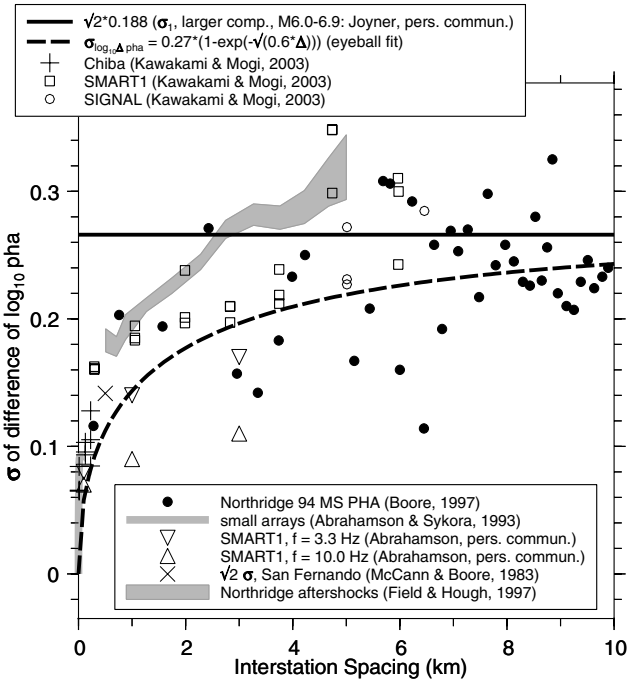

Figure A1. Standard deviation of difference of log of the larger peak horizontal acceleration as a function of interstation spacing. This provides the function $F(\Delta)$ referred to in the Appendix.

U.S. Geological Survey, MS 977
345 Middlefield Road
Menlo Park, California 94025
boore@usgs.gov, jtinsley@usgs.gov, dponti@usgs.gov

Manuscript received 17 September 2002.